TOWARDS ESTIMATING WATER COLUMN PROPERTIES USING AMBIENT NOISE INTERFEROMETRY IN THE DEEP OCEAN

John Ragland[a], Shima Abadi[a,b]

[a]Department of Electrical and Computer Engineering, University of Washington, Seattle WA 98195
[b]School, of Oceanography, University of Washington, Seattle WA 98195

John Ragland
jhrag@uw.edu
Paul Allen Center - AE100
Box 352500
185 Stevens Way Seattle, WA 98195-2500

Abstract: *The cross-correlation of stochastic ambient noise between two sensors can, under the right conditions, converge to an estimate of the Green's function between the two sensors. This passively estimated Green's function is referred to as the empirical Green's function. The Ocean Observatories Initiative (OOI) has 11 hydrophones that constantly record ambient sound in the ocean and makes the data publicly available. This observatory provides an opportunity to investigate ambient noise interferometry in the deep ocean. In this paper, two OOI bottom mounted hydrophones in the north-east Pacific, separated by 3.2 km and located at a depth of 1500 m are used to investigate the possibility of using passively estimated multi-path acoustic arrivals for measuring water column properties. Previous work has shown that the empirical Green's function between these hydrophones reliably contain peaks that correspond to multiple acoustic propagation paths throughout six years of analysed data. These peaks have the potential to be used for estimating information about the water column, such as sound speed or temperature. In this paper, the empirical Green's functions calculated for these two hydrophones will be used to estimate multi-path arrival times between the two hydrophones. Additionally, the accuracy of these arrival times will be quantified. The passively estimated arrival times will then be compared to simulated arrival times. Using acoustic simulations, the effects of sound speed fluctuation, and changing hydrophone geometry will be investigated and compared to the passively estimated arrival times. [work supported by ONR]*

Keywords: *ambient sound, cross-correlations, noise interferometry, coherent ambient sound, passive tomography*

1. INTRODUCTION

Ambient noise interferometry is a technique that uses coherent ambient sound to illuminate the acoustic propagation between sensors passively [1]–[7]. This estimate of acoustic propagation can then be used to estimate water properties, such as flow velocity, temperature, or mode shapes [8]–[13]. A recent paper [14] utilized ocean observatories initiative (OOI) hydrophones bottom mounted at 1500 m and separated by 3 km to reliably detect multipath propagation between the hydrophones in the deep ocean. In [15], the ambient sound scape measured by the OOI hydrophones and used as sources of opportunity for [14] is characterized. In [16] the contributions of surface source locations are experimentally explored using a seismic survey. The multi-path arrivals that are discussed in [14] traverse the entire water column and could potentially be used to estimate deep ocean temperature. In this paper, we will present continued work towards leveraging the OOI hydrophones to sense deep ocean temperatures and to further develop the capabilities of the technique of ambient noise interferometry. First, we will characterize the coherence of different multipath arrivals as a function of frequency. Second, we will look at the estimated arrival time of one of the multi-path peaks demonstrated in [14] over eight years of available data and compare it to simulated arrival times. Last, we will discuss the results of the study.

In section 2, the methods for calculating the noise cross-correlation function (NCCF), estimating arrival times from the NCCF, and simulating acoustic propagation are presented. In section 3, the results of the study are presented. Lastly, in section 4, the results are discussed.

2. METHODS

The methods used to calculate the noise cross-correlation function (NCCF), estimate arrival times from the NCCF, and simulate acoustic propagation between the sensors is presented in the following sections. A map of the two hydrophone locations is shown in Figure 1 (a).

2.1 Calculating the cross-correlation

The processing that we use to calculate the noise cross-correlation function (NCCF) is identical to processing used in [14]. We take a 30 second segment of data, filter it between 1 and 90 Hz using a 4^{th} order zero-phase Butterworth filter, clip the data to 3 times the standard deviation for a given hour of data, and then frequency whiten the data. This is done by windowing the segment with a Hann window and then replacing the magnitude in the frequency domain with the magnitude response of the Butterworth filter, preserving the phase information. These 30 s pre-processed data segments are then cross correlated together between the two sensors and the 30 second estimate of the correlation between the sensors is averaged together for a given averaging time. In [14], we characterized the emergence of the empirical Green's function as a function of averaging time and studied the 201 hour NCCF stack. This represents 201-hour average NCCFs consecutively calculated throughout the eight years of data analysed. In this work, we will continue to study the 201-hour NCCF stack.

2.2 Arrival time estimation

As explained in section 3.1, the frequency range where the NCCF estimate is above the incoherent noise floor is different for the various peak arrivals. To estimate the arrival time of

a specific, multi-path arrival time, the NCCF is first filtered to the cut-off frequencies given in Figure 2 using a zero-phase, 4th order Butterworth filter. Then the magnitude of the Hilbert transform is used to estimate a given arrival time.

Due to the small fluctuations in arrival time that are caused by changes in the environment, sub-time bin interpolation is needed to resolve changes in arrival times. The technique of quadratic peak interpolation is used to estimate the arrival times [17]. A 20 time-bin window around the expected arrival time is considered, and the location of the largest amplitude is computed. Along with the two adjacent time bins, the amplitude and locations of the largest amplitude time bin is used to estimate the arrival time of the peak.

2.3 Acoustic Simulation

Acoustic propagation between the two hydrophones is simulated using the method of normal modes [18, p. 260] and is calculated with KRAKEN [19]. The environment is simplified to be range independent, with the two hydrophones located at the same depth. The ocean depth is set to 1525 m, and the two hydrophones are placed at 1524 m, and separated by 3.202 km. The simulated TDGF is sampled for 30 seconds at 200 Hz and the result is filtered between 1-90 Hz. To estimate arrival times from the simulated TDGF, the same process described in section 2.2 is used.

To characterize the effects of changing temperature and salinity, sound speed information is obtained from HYCOM[1]. To characterize the effects of depth changes due to the inflation and deflation of the axial seamount volcano [20] and tidal changes, pressure data from the two OOI site locations is used. The effects of depth and temperature are assumed to be separable.

To simulate the effect of temperature and salinity changes in the water column, the 1-day average sound speed profile was calculated from HYCOM temperature and salinity data at (45.944335 -129.990713), which is 325 m from the midpoint between the two hydrophones. The time-domain Green's function was then simulated for each day. Figure 1(b) shows the first 400 m of the HYCOM sound speed profile from 2015 to 2023. Figure 1(d) shows the simulated TDGF for a single day.

To simulate the effect of depth changes, the time-domain Green's function was simulated for depth changes of 1 to 5 meters for each hydrophone. The arrivals times from this simulation are shown in Figure 1(e). Since the changes to depth are small relative to the hydrophone separation and ocean depth, the effect of depth changes is linear. A linear regression model is fit to the simulated changes in arrival time with an R2 score of 0.9956. This allows for the individual pressure measurements from each sensor to be used to characterize the change in arrival time due to changes in depth for the two hydrophones.

[1] https://www.hycom.org/

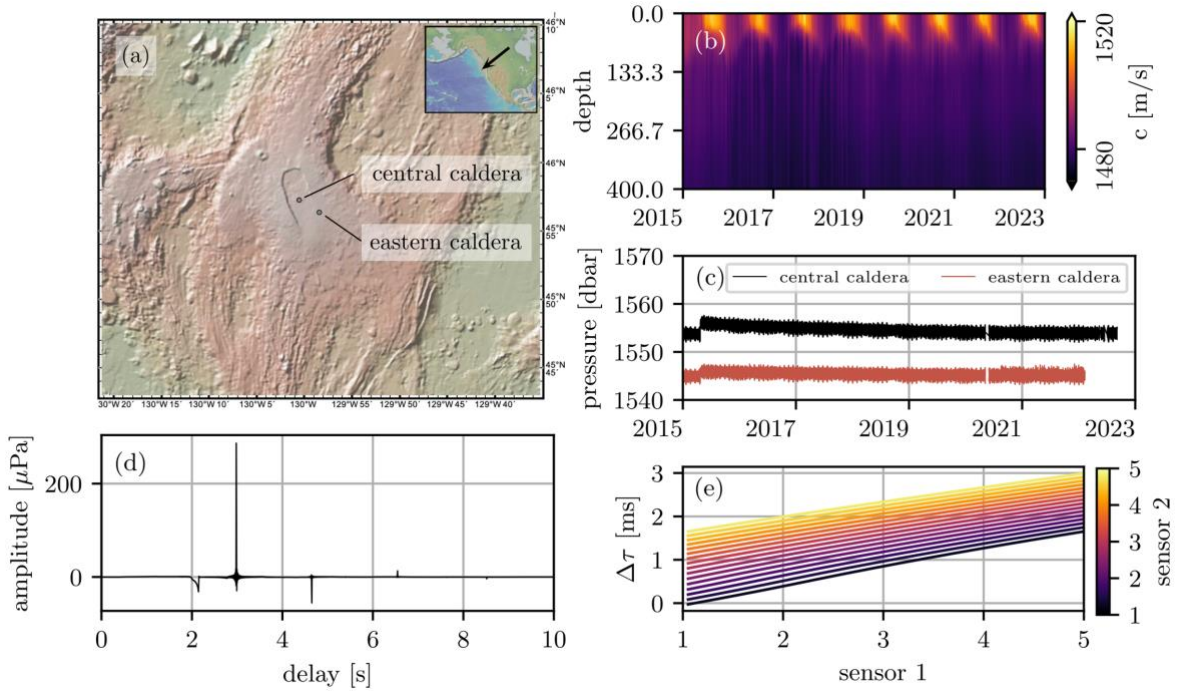

Figure 1: (a) Map of two OOI hydrophones used for this study. (b) First 400 meters of the sound speed profile computed with HYCOM temperature and salinity data. (b) Pressure data from the two hydrophone stations (d) Simulated time-domain Green's function for September 1, 2017. (e) Simulated effect of depth changes for the two sensors.

Even though, at the frequencies that we are simulating, the phase and group velocities have not converged, there is negligible spreading in time of the arrival times. This is due to the small separation of the hydrophones. Since there are discrete arrival times, it is useful to think of the acoustic propagation between the hydrophones in terms of ray paths. The peak at 2 seconds is due to the direct propagation between the two hydrophones. The peak at 3 seconds is due to a single reflection off of the surface of the ocean, and the peak at 4.6 seconds is due to two reflections off of the surface and one reflection off of the bottom. The arrivals are impulsive, but the fluctuations of arrival times due to temperature changes in the water column are still a function of frequency. Arrival times are used in this paper as a first order exploration of the forward consistency of the empirical Green's function that we estimate from ambient sound.

3. RESULTS

In this section, the coherency of different arrivals as a function of averaging time and frequency is presented. Additionally, the simulated arrival times using HYCOM and the estimated arrival time from the empirical Green's function are presented and compared.

3.1 Coherency

Inverting for water column properties requires estimating features of the time domain Green's function with a high level of accuracy. As shown in Figure 3(b), the fluctuations in arrival time due to environmental changes are on the order of 1 ms. To accurately sense arrival time changes due to changes in the environment, the signal-to-noise (SNR) ratio needs to be sufficiently large. In this section we investigate the SNR between coherent and incoherent sound as it changes with frequency and averaging time to better inform the estimates of the

empirical Green's function. We will characterize the frequency band where the signal-to-noise ratio is positive in dB, and only use this frequency band for arrival time estimates.

Ambient sound recorded by an array of sensors can be understood as a combination of coherent and incoherent sound. Coherent energy is the energy that propagates through the environment and is recorded by all the sensors. Incoherent sound is due to energy that is not recorded by all sensors and is either due to local sound sources or sensor self-noise. The technique of ambient noise interferometry utilizes diffuse, coherent, ambient sound to illuminate the acoustic propagation between sensors.

In practice, the coherent component of the ambient sound is buried in the incoherent noise and, to increase the signal to noise ratio of the empirical Green's function, the estimated coherence must be averaged over time. Assuming that the environment and source distribution are stationary, the coherent component does not change between samples of correlation. However, the stochastic fluctuations of the incoherent component will cancel out with increased averaging time.

Due to attenuation that is caused by scattering and absorption, coherent energy decreases with increasing frequency. This attenuation can be modelled as decreasing log-linearly. Figure 2 shows the distribution of windows of the NCCF corresponding to different arrival times in the frequency domain throughout the eight years of data analysed. A bilinear model is proposed to explain the patterns present in the data and is fit to minimize least squared error. The slope of the line-segment on the right is fixed to zero and the slope of the line-segment on the left and the intersection point of the lines are the model parameters that are fit. The model is fit between 5 and 80 Hz. The line segment on the right represents the broadband, incoherent noise that decreases with increasing averaging time. The line segment on the left represents the coherent energy that decreases log-linearly with increasing frequency. The intersection of the two lines represents the frequency where the signal-to-noise ratio between coherent and incoherent sound is 0 dB. Figure 2 shows the peak spectrums for 201 hours of averaging.

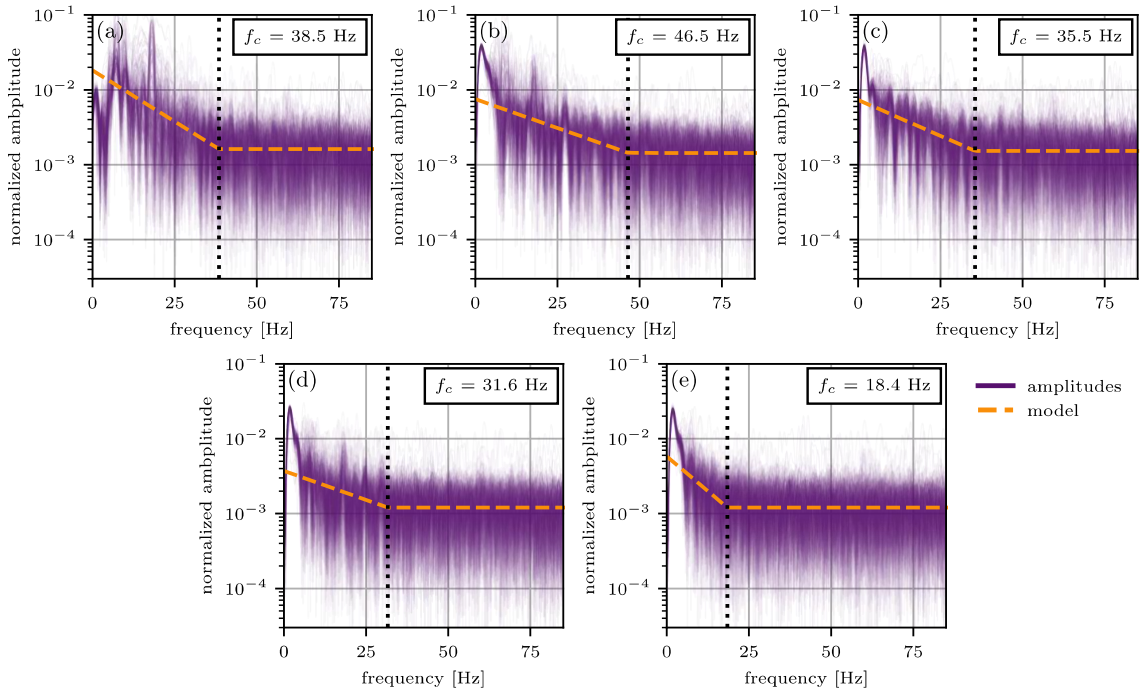

Figure 2: spectrum of different arrival peaks. (a) direct path lag (b) surface reflection lag (c) surface reflection lead (d) surface-bottom-surface reflection lag (e) surface-bottom-surface reflection lead

There is a large peak below 5 Hz for the four arrivals that reflect off the surface or bottom. This large peak is likely due to local wind sound. Since it is present only in the reflected arrivals, it is due to sound that is propagating at steep angles in the water column. As mentioned in section 2.2, the results of this section are used to band limit the empirical greens

function to the frequency bands that have coherent energy for a given arrival. In future work, we plan to use this characterization of the SNR to inform error bounds on estimated features from the empirical Green's function, such as arrival times.

3.2 Simulated and estimated arrival times

Figure 3 (a) shows the simulated relative arrival time change due to the depth changes. Figure 3(b) shows the simulated arrival time due to temperature fluctuations at a resolution of one day and the depth adjusted arrival time in red. Figure 3 (c) shows the estimated arrival times from ambient sound and the simulated arrival times for 201 hours of averaging.

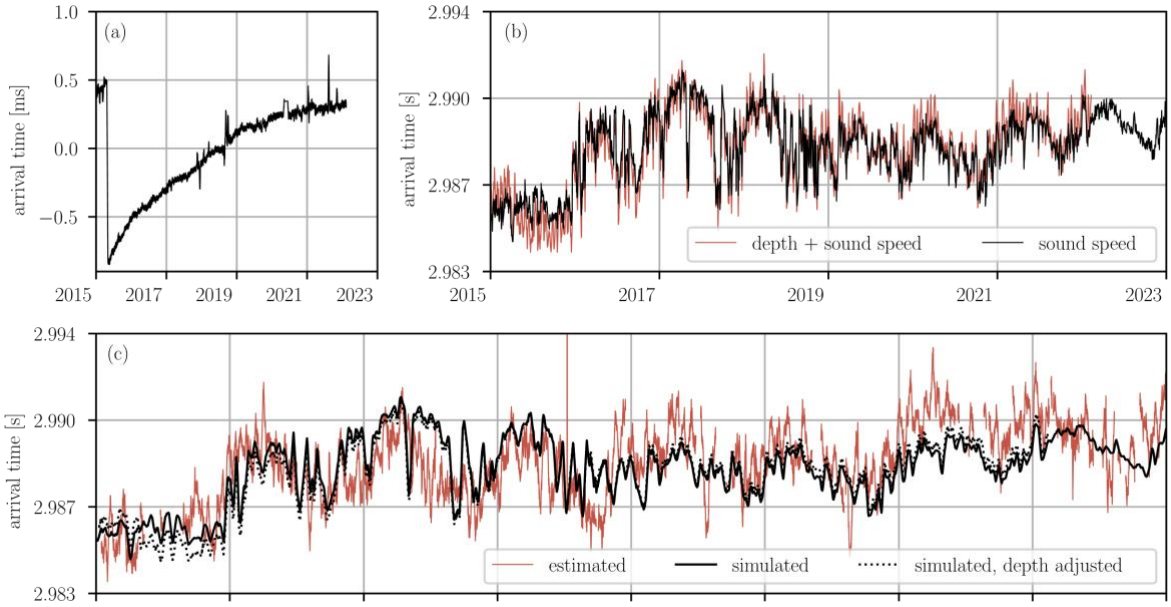

Figure 3: (a) simulated change in arrival time due to the depth changes of the two hydrophones at 1 hour resolution. (b) arrival time of surface reflection peak between simulated with HYCOM data. (c) 201 hour average arrival time estimated with ambient sound (red), 201 hour average arrival time simulated with HYCOM temperature and salinity data (black), and 201 hour average arrival time simulated with HYCOM and adjusted for depth changes (black dashed)

4. DISCUSSION

As seen in Figure 3, the arrival time estimates align with the simulated arrival times decently well. There is a strong annual feature in the estimated arrival times that aligns with the seasonal changes in temperature that effect the simulated arrival time. In 2015, the ocean was uncharacteristically warm (Figure 1(b)), resulting in a shorter arrival time. It seems that the arrival times estimated from ambient sound in the ocean are accurate enough to capture this feature in the water column. Since we don't have an in-situ measurement of temperature and salinity at this location, it is difficult to characterize if the discrepancies between estimated and simulated arrival times are due to inaccuracies in the estimated values, or simulated values. In future work, the error of estimated arrival times could be characterized using the signal-to-noise ratio, and the different levels of coherent energy with changing frequencies could be utilized to acquire more accurate estimates of the environment. Additionally, utilizing all the available arrival times would allow for 4 independent measurements of the water column.

In this work, bottom mounted hydrophones in the caldera of the axial seamount volcano were utilized to estimate acoustic propagation between the hydrophones. The coherent energy as a function of averaging time and frequency were examined for 5 reliably detected arrivals. This information was then used to inform how we estimate arrival times. The estimated arrival

time for the surface reflection, lag peak was estimated throughout 8 years of data analysed and compared to simulated arrival times using HYCOM and depth information of the hydrophones. The estimated arrivals have a clear annual fluctuation that aligns with the annual fluctuations in the simulated arrival times that are due to seasonal changes in temperature of the water column. This represents the first time that multi-path arrivals in the deep ocean have been measured using the technique of ambient noise interferometry.

ACKNOWLEDGEMENTS
Work supported by the Office of Naval Research grant number N00014-19-1–2644.

REFERENCES

[1] **P. Roux and W. A. Kuperman**, Extracting coherent wave fronts from acoustic ambient noise in the ocean, *The Journal of the Acoustical Society of America*, vol. 116, no. 4, pp. 1995–2003, Oct. 2004, doi: 10.1121/1.1797754.

[2] **R. L. Weaver and O. I. Lobkis**, Diffuse fields in open systems and the emergence of the Green's function (L), *The Journal of the Acoustical Society of America*, vol. 116, no. 5, pp. 2731–2734, Nov. 2004, doi: 10.1121/1.1810232.

[3] **K. G. Sabra, P. Roux, and W. A. Kuperman**, Arrival-time structure of the time-averaged ambient noise cross-correlation function in an oceanic waveguide, *The Journal of the Acoustical Society of America*, vol. 117, no. 1, pp. 164–174, Jan. 2005, doi: 10.1121/1.1835507.

[4] **P. Roux and M. Fink**, Green's function estimation using secondary sources in a shallow water environment, *The Journal of the Acoustical Society of America*, vol. 113, no. 3, pp. 1406–1416, Feb. 2003, doi: 10.1121/1.1542645.

[5] **P. Roux, K. G. Sabra, W. A. Kuperman, and A. Roux**, Ambient noise cross correlation in free space: Theoretical approach, *The Journal of the Acoustical Society of America*, vol. 117, no. 1, pp. 79–84, Jan. 2005, doi: 10.1121/1.1830673.

[6] **O. A. Godin, N. A. Zabotin, and V. V. Goncharov**, Ocean tomography with acoustic daylight, *Geophysical Research Letters*, vol. 37, no. 13, 2010, doi: https://doi.org/10.1029/2010GL043623.

[7] **O. A. Godin**, On the possibility of using acoustic reverberation for remote sensing of ocean dynamics, *Acoust. Phys.*, vol. 58, no. 1, pp. 129–138, Jan. 2012, doi: 10.1134/S1063771012010101.

[8] **K. F. Woolfe, S. Lani, K. G. Sabra, and W. A. Kuperman**, Monitoring deep-ocean temperatures using acoustic ambient noise, *Geophysical Research Letters*, vol. 42, no. 8, pp. 2878–2884, 2015, doi: https://doi.org/10.1002/2015GL063438.

[9] **L. G. Evers, K. Wapenaar, K. D. Heaney, and M. Snellen**, Deep ocean sound speed characteristics passively derived from the ambient acoustic noise field, *Geophysical Journal International*, vol. 210, no. 1, pp. 27–33, Jul. 2017, doi: 10.1093/gji/ggx061.

[10] **X. Zang, M. G. Brown, and O. A. Godin**, Waveform modeling and inversion of ambient noise cross-correlation functions in a coastal ocean environment, *The Journal of the Acoustical Society of America*, vol. 138, no. 3, pp. 1325–1333, Sep. 2015, doi: 10.1121/1.4928303.

[11] **O. A. Godin, M. G Brown, N. A. Zabotin, L. Y. Zabotina, and N. J. Williams**, Passive acoustic measurement of flow velocity in the Straits of Florida, *Geoscience Letters*, vol. 1, no. 1, p. 16, Dec. 2014, doi: 10.1186/s40562-014-0016-6.

[12] **T. W. Tan and O. A. Godin**, Passive acoustic characterization of sub-seasonal sound speed variations in a coastal ocean, *The Journal of the Acoustical Society of America*, vol. 150, no. 4, pp. 2717–2737, Oct. 2021, doi: 10.1121/10.0006664.

[13] **F. Li, X. Yang, Y. Zhang, W. Luo, and W. Gan**, Passive ocean acoustic tomography in shallow water, *The Journal of the Acoustical Society of America*, vol. 145, no. 5, pp. 2823–2830, May 2019, doi: 10.1121/1.5099350.

[14] **J. Ragland and S. Abadi**, Long-term noise interferometry analysis in the northeast Pacific Ocean, *The Journal of the Acoustical Society of America*, vol. 149, no. 4, pp. A90–A90, Apr. 2021, doi: 10.1121/10.0004609.

[15] **J. Ragland, F. Schwock, M. Munson, and S. Abadi**, An overview of ambient sound using Ocean Observatories Initiative hydrophones, *The Journal of the Acoustical Society of America*, Jan. 2022.

[16] **J. Ragland and S. Abadi**, Exploring surface source contributions to ocean ambient noise interferometry with airgun shots, vol. The Journal of the Acoustical Society of America, 2022.

[17] **J. O. Smith**, *Spectral Audio Signal Processing*. W3k Publishing, 2011. Accessed: Jun. 10, 2021. [Online]. Available: https://ccrma.stanford.edu/~jos/sasp/

[18] **L. E. Kinsler, A. R. Frey, A. B. Coppens, and J. V. Sanders**, *Fundamentals of Acoustics*. John Wiley & Sons, 2000.

[19] **M. B. Porter**, The KRAKEN Normal Mode Program, NAVAL RESEARCH LAB WASHINGTON DC, May 1992. Accessed: Oct. 07, 2021. [Online]. Available: https://apps.dtic.mil/sti/citations/ADA252409

[20] **W. W. Chadwick Jr., W. S. D. Wilcock, S. L. Nooner, J. W. Beeson, A. M. Sawyer, and T.-K. Lau**, Geodetic Monitoring at Axial Seamount Since Its 2015 Eruption Reveals a Waning Magma Supply and Tightly Linked Rates of Deformation and Seismicity, *Geochemistry, Geophysics, Geosystems*, vol. 23, no. 1, p. e2021GC010153, 2022, doi: 10.1029/2021GC010153.